Title

Spectroelectrochemical Photoluminescence of Trap States in H-Treated Rutile TiO2 Nanowires: Implications for Photooxidation of Water

Journal

The Journal of Physical Chemistry C, 120(6)

ISSN

1932-7447

Authors

Rex, Riley E
Yang, Yi
Knorr, Fritz J
et al.

Publication Date

2016-02-18

DOI

10.1021/acs.jpcc.5b11231

Peer reviewed

THE JOURNAL OF PHYSICAL CHEMISTRY C

Article

pubs.acs.org/JPCC

Spectroelectrochemical Photoluminescence of Trap States in H-Treated Rutile TiO_2 Nanowires: Implications for Photooxidation of Water

Riley E. Rex,[†] Yi Yang,[‡] Fritz J. Knorr,[†] Jin Z. Zhang,[‡] Yat Li,[‡] and Jeanne L. McHale*[,†]

[†]Materials Science and Engineering Program and Department of Chemistry Washington State University, Pullman, Washington 99164-4630, United States

[‡]Department of Chemistry and Biochemistry University of California, Santa Cruz, Santa Cruz, California 95064, United States

Supporting Information

ABSTRACT: Photoluminescence (PL) spectroscopy of intra-bandgap trap states is used to investigate the mechanism of photocatalytic water oxidation in pristine and hydrogen-treated rutile TiO_2 nanowires. H-treated nanowires annealed at 350 °C were previously shown to be superior to pristine nanowires for the photoelectrochemical evolution of oxygen from water, owing to more efficient charge separation and carrier transport. The present work examines the near-IR PL of rutile nanowires under applied electrochemical potential in order to address the possible influence of hydrogen treatment on electron or hole traps and their role in water oxidation. It is concluded that the near-IR PL of rutile nanowires, identical to that of bulk and conventional nanocrystalline rutile, arises from the radiative recombination of trapped electrons with valence band holes and that valence band holes, rather than trapped holes, are more likely responsible for water oxidation. The shape and intensity of the near-IR PL is found to be invariant to H-treatment and thus does not arise from traps introduced by annealing in H_2, such as oxygen vacancies. Instead, H-treatment influences carrier transport and the recombination processes which compete with reductants for hole consumption. The role of contacting solvent, water versus wet acetonitrile, is shown to exert a strong influence on whether deep traps are occupied isoenergetically (from the potentiostat) or inelastically (by photogenerated electrons in the conduction band).

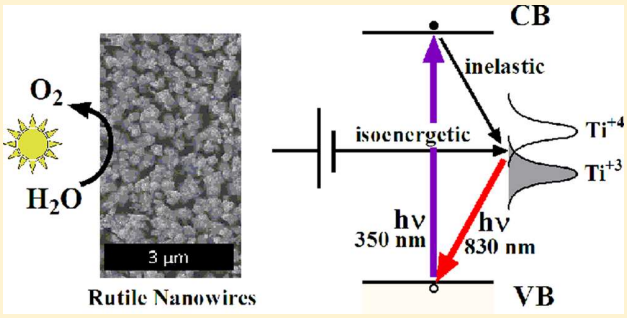

INTRODUCTION

Nanostructured titanium dioxide has been widely investigated as a promising material for renewable energy applications including dye-sensitized solar cells and photoelectrochemical water splitting due to its low cost, relative abundance, corrosion resistance, and favorable positions of the valence and conduction bands.[1−3] Rutile photoanodes have been shown to be effective at oxidizing water,[4,5] and more recently, some of us have demonstrated a solar-to-hydrogen efficiency of 1.1% from hydrogen-treated rutile nanowires (RNWs).[6] In that work, it was shown that annealing RNWs in a reducing H_2 environment results in a significant improvement in efficiency compared to untreated RNW photoanodes. The improvement in H-treated samples was attributed to increased donor density leading to improved charge transport as evidenced by increased photocurrent and greatly improved incident-photon-to-current conversion efficiency (IPCE) in the ultraviolet region.[6] The relationship between charge carrier trap states and the performance enhancement observed in H-treated rutile photoanodes was recently investigated using EPR, time-resolved fluorescence, and femtosecond transient absorption.[7] It was concluded that H-treatment introduces oxygen vacancies with energies 0.3 eV below the conduction band (CB) edge, giving rise to weak blue PL. Hydrogen treatment thus improves transport by introducing donor states that raise the Fermi level. In addition, transient absorption spectroscopy of hole and electron traps has revealed that recombination is reduced in H-treated as compared to pristine RNWs.[8] This effect was attributed to a significant band bending in the radial direction, made possible by high donor densities in the H-treated nanowires.[9]

In addition to the weak visible PL observed in ref 7, more intense near-IR (but still rather weak) PL of rutile at about 840 nm is well-known in both bulk[10] and nanocrystalline[11] samples. Nakato et al.[12] have assigned this PL to recombination of conduction band electrons with holes trapped at 3-fold coordinated (normal) oxygen atoms, O_{3c}, on the surface of rutile (110) or (100), where they have slightly different energies. They have proposed that this surface-trapped hole, found in the middle of the 3 eV rutile band gap, catalyzes the

Received: November 16, 2015
Revised: January 27, 2016
Published: January 29, 2016

DOI: 10.1021/acs.jpcc.5b11231
J. Phys. Chem. C 2016, 120, 3530−3541

photooxidation of water in a mechanism initiated by the nucleophilic attack of O_{3c} by a water molecule. In this picture, water-oxidation competes with PL for consumption of trapped holes, and surface roughening that accompanies water oxidation leads to more favorable hole transfer to water. It has also been proposed that chemisorbed water molecules trap valence band (VB) holes to form hydroxyl radicals $OH^{\bullet}$.[13] Surface hydroxide groups have long been identified as possible hole traps on TiO_2[14] and the resulting $OH^{\bullet}$ radicals can potentially serve as photooxidants. More recently, Imanishi et al.[15] have reported further studies supporting the idea that trapped holes at O_{3c}, which would otherwise recombine with CB electrons to produce near-IR PL, are responsible for water oxidation. In contrast, Li et al.[16] also examined the same near-IR PL of rutile, but they attribute it to recombination of trapped electrons, of unspecified chemical nature, with valence band holes. Thus, the very nature of the near-IR PL is central to understanding the photocatalytic properties of rutile.

The role of trapped versus free carriers in photoredox processes on TiO_2 is an important consideration for optimizing the efficiency of processes such as solar-to-hydrogen conversion. Salvador et al.[17,18] distinguish direct hole transfer from the valence band to a reductant, which is favored when the latter is specifically adsorbed on the surface, as opposed to indirect hole transfer from trap states such as $OH^{\bullet}$. Indirect hole transfer is an isoenergetic process which may predominate for species not specifically adsorbed on the surface. Alternatively, the rate of interfacial electron transfer can be cast in terms of Marcus-Gerischer theory and depends on the overlap of the donor state distribution with the density of states for empty levels of the semiconductor.[19,20] Since four photogenerated holes are required to generate a single O_2 molecule, the role of trapped holes might be significant, provided they have sufficient driving force for substrate oxidation. Regardless of the mechanism, hole transfer from TiO_2 to water in the absence of electron scavengers is unfortunately much slower than electron−hole recombination.[21] Determination of the spatial and energetic distribution of trap states that participate in electron−hole recombination and/or redox processes is thus imperative. Another obstacle to efficient water oxidation is the existence of overpotentials as large as 0.7 V.[22] A better understanding of the energies of trap states on an electrochemical scale, as well as the kinetic barriers to occupying them, is important to elucidating the mechanism of TiO_2 as a photoanode. Studies of trap states and associated defects in rutile have included EPR,[23] infrared spectroscopy,[24] theory,[25,26] photoemission spectroscopy,[27] EELS,[28] STM,[29] and spectroelectrochemistry.[30] However, some of these are high vacuum techniques which, despite their elegance, do not directly reveal properties of TiO_2 electrodes in working photoelectrochemical cells.

In past work, we have used spectroelectrochemical photoluminescence (SEPL) to determine the nature and electrochemical energies of trap states in nanocrystalline anatase TiO_2 films.[31,32] By examining the PL of nanocrystalline films of TiO_2 under Fermi level control, SEPL enables the investigation of trap states and recombination processes at the surface under conditions relevant to photoelectrochemical applications. The technique has also been used by another group to investigate the luminescent trap states of nanocrystalline ZnO.[33] Based on our SEPL work and studies of the PL at open circuit,[34,35] we have assigned the broad visible PL of anatase TiO_2 to a superposition of two types of radiative transitions: recombination of mobile electrons with trapped holes and recombination of electrons trapped as Ti^{3+} with valence band holes. Using SEPL, we found that the broad visible PL of anatase shifted to the blue as the Fermi level was raised. Numerical modeling of the potential dependent PL spectra revealed the component spectra and onset potentials for occupying two distinct electron trap state populations, emitting in the yellow and red, and a third spectral component associated with the recombination of conduction band electrons with trapped holes, peaking at a green wavelength. SEPL revealed the energies of trap occupation on an electrochemical scale, and it was shown that an overpotential exists for occupying electron traps in the presence of water versus acetonitrile (ACN).

In this work, we apply SEPL to examine the PL spectra of RNW trap states as a function of applied potential, pH, and in nonaqueous electrolyte. We compare the SEPL of pristine nanowires to that of nanowires annealed in H_2 at 350 and 450 °C (H350 and H450, respectively) to investigate the basis for superior performance of the H350 sample in water oxidation. Comparison of the potential-dependent photocurrents to the SEPL reveals the nature of the PL and the energies for populating electron traps. The results are used to address the possible role of the luminescent traps in water oxidation, and the role of contacting solvent electrolyte on trap occupancy and electron−hole recombination. Unlike the PL of nanocrystalline anatase, the near-IR PL of rutile nanowires does not shift with electrochemical potential or contacting solvent, nor does it vary in shape or wavelength with H-treatment. Nevertheless, it will be seen that the potentials for occupying traps vary with pH and are different for aqueous and nonaqueous electrolyte. Comparison of the potential dependence of the PL and the anodic photocurrent reveal the nature of the trap states involved and provides insight into the mechanism of water photooxidation.

EXPERIMENTAL SECTION

The rutile nanowire (RNW) films were prepared as described previously.[6] The films consist of densely packed nanowires growing vertically on conductive FTO glass in the <001> direction with predominately {110} surfaces. As-grown samples were then either used as is, labeled "pristine", or annealed in H_2 at 350 or 450 °C. The hydrogen-treated samples are labeled H350 or H450 for their treatment temperature. The nanowire morphology can be seen in the Supporting Information, Figure S1. The nanowire films prepared via this method were previously confirmed to be rutile phase with XRD and high-resolution TEM. The specific films used in this study were confirmed rutile using Raman spectroscopy as seen Figure S2.

Aqueous electrolyte solutions of 0.2 M $NaClO_4$ in 18 MΩ H_2O were prepared at pH values of 1.8, 6.1, 9.5, and 12.0 using perchloric acid, phosphate buffer, carbonate buffer, and NaOH, respectively. All buffers and electrolytes were sodium salts, unless otherwise noted. Nonaqueous electrolyte solutions were prepared in Optima-grade acetonitrile (ACN) from Fisher Scientific. The ACN had a reported water content of 0.008% and the $NaClO_4$ waters of hydration contributed 0.2 M water to the ACN electrolyte solution. To test the influence of residual water in ACN, additional experiments were done using ACN electrolyte solution dried by 3A molecular sieves, and using anhydrous $LiClO_4$ instead of $NaClO_4$ to avoid waters of hydration. All solvents were degassed prior to solution preparation.

DOI: 10.1021/acs.jpcc.5b11231
J. Phys. Chem. C 2016, 120, 3530−3541

Photoluminescence measurements with Fermi level control were carried out as described previously.[31,32] Briefly, excitation at 350.7 nm was provided by a BeamLok 2060 Spectra-Physics krypton ion laser. The beam was passed through a 350 nm interference bandpass filter to remove plasma lines. The samples were arranged to measure the front face emission of light using an excitation beam which impinges on the sample in a near normal geometry. The emitted light was collected with an objective lens, filtered with a 385 nm long-pass filter and focused into an Acton SpectroPro 2300i monochromator equipped with a 150 g/mm grating, and a thermoelectrically cooled CCD (Princeton Instruments Spec10). Incident light intensity at the sample was typically 100 mW/cm^2. Note that this is much larger than typical intensities used in photoelectrochemical measurements and is necessary owing to the apparent low quantum yield of rutile PL. At the powers used here, the efficiency of water oxidation is low as a result of enhanced recombination.[21] Exposure times were 4 s. Intensities in Figures 1−5 are listed as counts collected in this 4 s interval. To obtain reproducible PL intensities, a fixed illumination geometry and incident laser power were used for all the measurements. For SEPL, applied potentials were controlled by a BAS100A electrochemical analyzer and a 3-electrode setup. The working electrode and counter electrode were the rutile nanowire films and platinum wire, respectively. The reference electrode in aqueous solutions was 3 M NaCl Ag/AgCl. The reference electrode in acetonitrile was a nonaqueous Ag/Ag$^+$ reference electrode from BASi. The potential of Ag/Ag$^+$ in 0.2 M $NaClO_4$ acetonitrile was determined using cyclic voltammetry of the ferrocene/ferrocenium redox couple as an external standard. All potentials reported herein are referenced to Ag/AgCl (3 M NaCl), which is +0.209 V versus NHE. SEPL measurements were carried out starting at positive potentials and progressing to negative potentials in 50 mV steps and are reported as maximum PL intensity vs electrochemical potential. These are referred to herein as SEPL profiles. Repeat measurements at the most positive potentials were obtained at the end of each series to test reversibility. At each potential step, the system was allowed to equilibrate for 20 s before recording the current and subsequently recording the PL spectrum. Further current measurements were made as a function of potential using cyclic voltammetry (CV) with a scan rate of 100 mV/s.

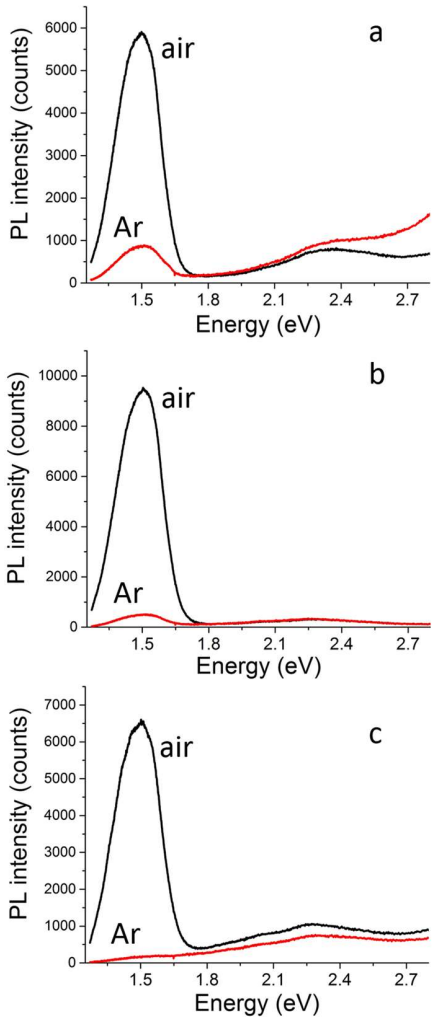

Figure 1. PL of pristine (a), H350 (b), and H450 (c) rutile NW in air (black) and Ar (red) environments.

RESULTS AND DISCUSSION

As seen in SEM images in the Supporting Information (SI), Figure S1, the RNWs are rectangular in shape with growth along the <001> direction, exposing mostly {110} surfaces, with average lengths of about 5 μm and oriented in the direction perpendicular to the conductive substrate on which they are grown. For the excitation/emission geometry used here, the incident light excited PL from the majority {110} surfaces as well as the top (001) surface.

Figures 1a−c show the PL spectra of pristine, H350, and H450 RNWs in air and in argon. The dominant PL from RNWs is a broad, near-infrared emission that peaks at 825 nm (1.5 eV).[10,11,36] This wavelength is intermediate between the peak at about 810 nm for the (110) surface and that at 840 nm for the (100) surface.[37] We are not aware of a measurement of the near-IR PL for a bulk rutile crystal exposing the (001) surface. In addition to the main peak at 1.5 eV, weak green PL at about 550 nm (2.3 eV) is also observed. This PL appears to be similar to that observed in mixed rutile-anatase films.[11] Due to its low intensity the green PL is emphasized less than the near-IR in this work, but we note that it could be assigned to oxygen vacancies as in past work on anatase nanocrystals, where green PL increased on vacuum annealing.[38] This weak visible PL was found to be rather irreproducible, and overlap with the visible PL of the conductive substrate was a problem for these samples. In addition, the well-known ability of O_2 and H_2O to adsorb at oxygen vacancies may result in variations in the green PL intensity.[39,40]

The photon energy of the near-IR PL indicates that the luminescent trap states are located in the middle of the 3.0 eV bandgap. Upon comparing the PL of pristine and H-treated RNW samples, we observed no change in the shape of the emission centered at 835 nm, indicating that these traps are not affected by the hydrogen treatment, as seen in Figure S3 of the SI. Furthermore, we observe no correlation between PL intensity at 835 nm and H-treatment, suggesting that the H-treatment does not significantly alter the number of near-IR luminescent surface traps. The effect of air versus argon on the near-IR PL intensity provides insight into the nature of the transition. This effect is opposite to what is observed for the visible PL of the anatase form of TiO_2, which is almost completely quenched in air at room temperature.[11,41] It is also

DOI: 10.1021/acs.jpcc.5b11231
J. Phys. Chem. C 2016, 120, 3530−3541

in contrast to previous work on conventional rutile nanoparticles where the near-IR PL was found to be relatively insensitive to the presence of air versus argon.[11] It is well-known that oxygen can scavenge electrons from TiO_2,[24,39,42,43] though this effect seems to be more frequently associated with anatase than with rutile (with the exception of ref 39). Assuming that O_2 does capture electrons from the CB of the nanowires, the results of Figure 1 argue for assigning the near-IR PL to the recombination of deeply trapped (midbandgap) electrons with VB holes. If the near-IR transition were the result of radiative recombination of CB electrons with trapped holes, air should have quenched rather than enhanced the intensity of PL. At open circuit, the Fermi level is higher than the energy of these traps and so they would already be occupied. When O_2 is present to scavenge photogenerated electrons from the CB, there is less competition for VB holes and the PL increases. In contrast, the higher-lying electron traps in anatase are populated through the conduction band such that interception of free photoelectrons by O_2 prevents PL from the recombination of trapped electrons with VB holes. The question remains as to why the "oxygen enhancement" effect was not observed previously when using conventional rod-shaped rutile nanoparticles.[11] One explanation is that the RNWs have more binding sites for O_2, which is known to adsorb at oxygen vacancies on rutile TiO_2(110).[44] Alternatively, better transport properties of RNWs compared to conventional rutile nanoparticles may be responsible for the different effects of oxygen on the PL. In either of these scenarios the effect of air on the PL would be expected to be greater for H-treated than pristine nanowires, and Figure 1 does display a trend of this type. Though O_2 is thermodynamically capable of scavenging electrons from rutile, it is apparent that it does so more efficiently for nanowires than for conventional nanoparticles. In order for adsorbed O_2 to scavenge photoelectrons from the conduction band, the time scale for electrons to diffuse from the illuminated part of the film to O_2 adsorption sites must be fast compared to electron–hole recombination. Improved carrier diffusion lengths and reduced recombination in RNWs, as compared to previously used 10 nm by 40 nm rutile nanoparticles, may explain why oxygen has a strong effect on the PL of rutile nanowires but little effect on that of rutile nanoparticles.[11]

To identify the effective electrochemical energy level of luminescent trap states in aqueous solutions, potential-dependent PL measurements were made in aqueous electrolyte solutions with four different pH values. Figure 2a–c shows the SEPL profiles for pristine rutile, H350, and H450 nanowires. The spectral shape of the near-IR emission does not change with applied potential, as shown in Figure S4 of the SI. The following analysis simply looks at intensity at the peak wavelength as a function of applied voltage. The intensity of PL emission at 835 nm is steady at a baseline value at the most positive potentials, and it then increases to reach a maximum at a potential approximately 200–300 mV below the CB edge indicated by the color-coded vertical lines in Figure 2. The CB values used here are obtained using the equation $E_{CB} = -0.16\ V - 0.059pH$ versus Ag/AgCl. We take the pH dependent flatband potential of nanocrystalline anatase as reported in ref 45 and, in accord with ref 46, adjusted it to account for 0.2 V less negative CB potential of rutile compared to anatase. (See also ref 47.) After the peak in intensity, the PL at 835 nm then rapidly decreases to zero as the applied potential becomes more negative and approaches the CB. This decrease in PL is

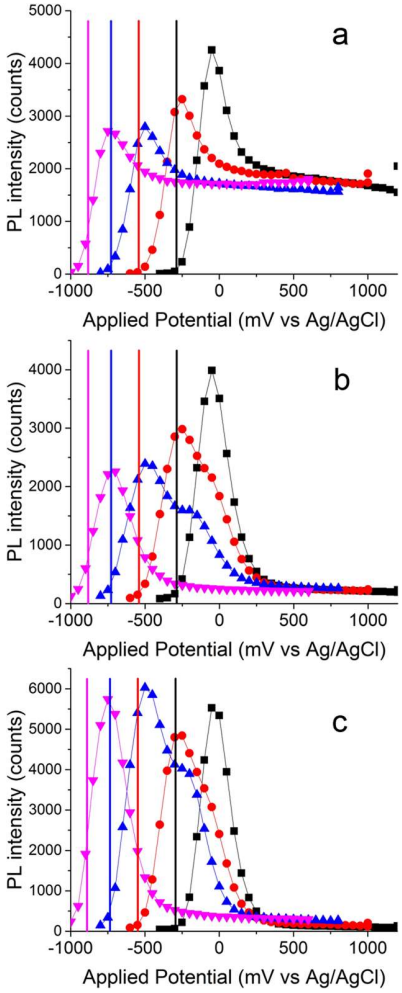

Figure 2. Photoluminescence intensity at 835 nm as a function of applied potential for (a) pristine, (b) H350, and (c) H450 rutile NW in 0.2 M $NaClO_4$ aqueous solutions pH 1.8 (black squares), pH 6.1 (red circles), pH 9.5 (blue triangles), and pH 12.5 (pink inverted triangles). The vertical lines represent the flat band potentials for rutile in aqueous solutions at their respective pH values. An additional data point was recorded at the most positive potential for each scan to test for reproducibility.

attributed to competition with nonradiative recombination, for which the rate increases as electrons are accumulated.[48] There may be an additional decrease in PL as the Fermi level moves above the conduction band edge owing to the blue-shift in the band gap energy.[49]

We note that, while the overall potential-dependent PL behavior was consistent and reproducible for multiple samples of H-treated and pristine films, the intensity of the PL plateau at positive potentials varied across samples. For example, in Figure 2a we see the intensity of the plateau for a pristine sample is at or above 50% of the maximum PL intensity, compared to less than 10% for H350 and H450 in Figure 2b,c, respectively. The intensity of the PL plateau is inversely proportional to the photocurrent at the associated applied potentials for comparable samples, as shown by Figure S5 in the SI. We note that a higher PL plateau, as in Figure 2a, is more commonly observed for pristine samples than for H-treated samples. The ability to directly populate or depopulate traps through variation of the applied potential is dependent on

DOI: 10.1021/acs.jpcc.5b11231
J. Phys. Chem. C 2016, 120, 3530–3541

the relative rates of carrier transport and recombination. The superior transport properties of the H350 and H450 samples, as compared to pristine RNWs, makes it easier to empty and fill traps as the applied potential is made respectively more positive or negative. Given that the Fermi level at open circuit is likely to lie a little below the CB minimum, electrons trapped in the middle of the band have to be pulled out as positive potential is applied. Less efficient transport in pristine RNWs compared to H-treated samples results in more frequent appearance of the plateau at positive potentials in the former. We found the occurrence of this plateau to be somewhat irreproducible. This observation could correlate to the well-known dependence of oxygen vacancy content on sample history and preparation,[50] and the resulting influence of these defects on transport.[41] In addition, rutile nanowires have been shown to undergo photocorrosion which causes the decay of photocurrent over time.[51] This photocorrosion might explain fluctuations in trap state density and thus PL intensity. Although beyond the scope of the present study, it has been reported recently that the photostability of rutile nanowires can be enhanced though surface treatments.[52]

We can envision several different mechanisms for the near-IR PL: recombination of trapped electrons with VB holes, recombination of CB electrons with trapped holes, recombination of a donor−acceptor pair,[33] or a molecularly based emission such as one associated with d−d transitions of an electron trapped as Ti^{3+}.[26] For the first of these, we would expect that, in the absence of an overpotential for populating trap states, the PL should increase as the Fermi level is raised (increasingly negative potential) through the energy of the trap state, which should be poised 1.5 V below the CB edge. It is apparent that for aqueous electrolyte the onset potential for the PL increase is more negative than expected on this basis. Alternatively, if the PL results from a hole trapped 1.5 V below the CB, the PL should have started off at a baseline value limited by the incident light intensity (number of photoholes) and simply decreased when the Fermi level is raised past the middle of the band gap. This is not what is observed either. However, when the electrolyte is acetonitrile (ACN) instead of water, a different SEPL profile is obtained and will be shown to provide insight into the nature of the PL transition.

As we have seen previously, the interaction between water and the TiO_2 surface can have a strong effect on the electrochemical energy level required to populate trap states and thus the potential-dependent PL in aqueous solutions.[32] Therefore, we tested the influence of water on the SEPL of RNWs by repeating the measurements using the relatively electrochemically inert solvent acetonitrile. Figure 3a−c shows the SEPL for pristine, H350 and H450 RNWs in nonaqueous environment. The shape of the near-IR PL spectrum is the same in water and in ACN, as seen in Figure S6 of the SI. Note that the data in Figure 3 were taken using ACN electrolyte containing about 0.2 M water. The most striking feature in the results in this solvent is the peak in PL near +500 mV and the rapid quenching of the PL as the applied potential approaches 0 mV vs Ag/AgCl. A second PL increase in ACN occurs between −300 and −500 mV with a subsequent peak and decrease near the estimated CB potential of −600 mV vs Ag/AgCl. Here we are applying the results of She et al.,[53] who found the CB potential in ACN that has not been extensively dried is approximately equivalent to that found in water at pH 7.8. Adjusting for the lower energy CB of rutile approximates the CB potential at −600 mV versus Ag/AgCl.[46] Thus, the PL peak

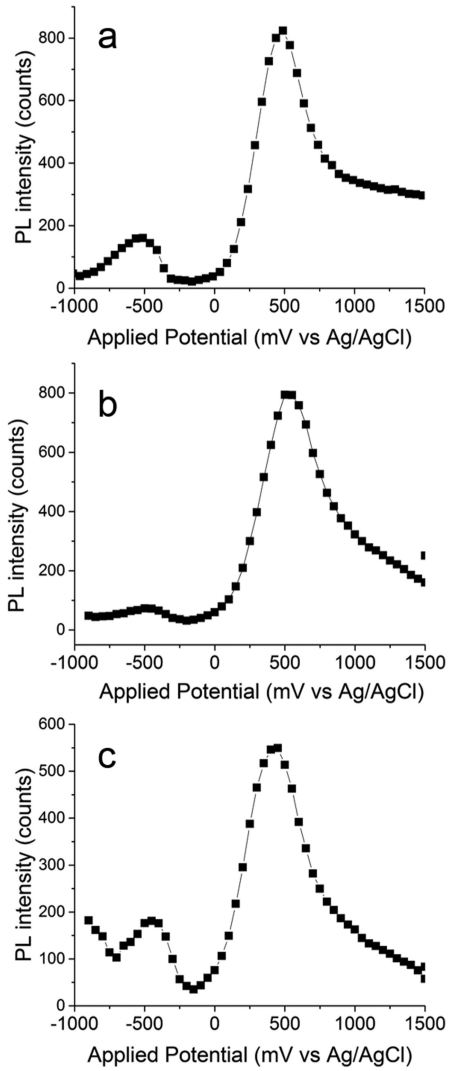

Figure 3. Photoluminescence intensity at 835 nm versus applied potential for (a) pristine, (b) H350, and (c) H450 rutile NW in 0.2 M $NaClO_4$ ACN.

at more negative potential appears to correspond to the single peak in the SEPL for RNWs in water, since in all cases the PL falls off as the CB potential is approached.

The presence of a second peak in the SEPL profile at positive potential in ACN but not water is similar to our previous results with mesoporous anatase TiO_2 films.[32] In these RNW samples, the increase in PL intensity 0.2−0.3 V below the CB seen in aqueous solutions does not match the 1.5 eV photon energy of the PL emission. Conversely, the SEPL peak at +0.5 V vs Ag/AgCl, observed in ACN, is about 1.1 eV below the CB edge. Compared to the SEPL data in the presence of water, this peak aligns more closely with the expected trap state position, i.e., near the middle of the 3.0 eV band gap. Due to this closer agreement between the spectroscopic and electrochemical energies, we suggest the SEPL data in ACN more accurately represents the energetic position of luminescent traps in RNW samples. We assign the two peaks in the SEPL for RNWs in acetonitrile to two mechanisms for filling of the midbandgap trap. The peak at positive potential represents the isoenergetic pathway for delivering carriers from the potentiostat to the trap state, while the peak at more negative potential results from

DOI: 10.1021/acs.jpcc.5b11231
J. Phys. Chem. C 2016, 120, 3530−3541

mobile carriers, in transport-limiting states just below the CB edge, which are captured inelastically by lower energy traps.

The uncertainty about whether the primary increase in PL observed at +0.75 mV vs Ag/AgCl in ACN is actually 1.5 V more positive than the CB potential may be compounded by the influence of residual water in the electrolyte solution. To address this, we repeated the nonaqueous SEPL experiment using 0.2 M anhydrous $LiClO_4$ as the electrolyte in ACN dried with 3A molecular sieves. As shown in Figure 4, the results are

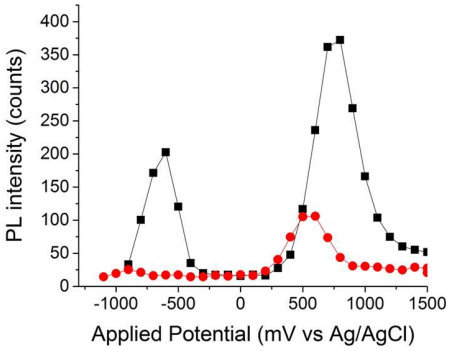

Figure 4. SEPL profile of H350 RNW in dry 0.2 M $LiClO_4$ ACN before (black) and after (red) adding 4% by volume dry EtOH.

similar to those of Figure 3 except that that the peak in PL intensity at positive potential is several hundred millivolts more positive than that for wet ACN. There is no corresponding change in the onset of the peak at more negative potential. The flatband potential for anatase TiO_2, and presumably also for rutile, is known to be more negative in dry ACN than in water and protic solvents, and to shift positively in the presence of Li^+ in aprotic solvent.[54] Since the SEPL peak at negative potential does not shift as a result of the small amount of water in the wet ACN electrolyte, we assume that the water content in this electrolyte is insufficient to move the CB to lower energy compared to dry ACN. There is some ambiguity, however, in the comparison of dry ACN containing $LiClO_4$ and wet ACN with $NaClO_4$ and 0.2 M water. If rutile TiO_2 is comparable to anatase, the removal of water might have caused the conduction band potential to shift negatively, while addition of Li^+ could result in a positive shift. The appearance of the negative potential SEPL peak at the same position in both electrolytes could result from a cancellation of these two effects. While more study of the effect of Li^+ versus Na^+ is warranted, the significant shift in the positive potential SEPL peak seems to be dominated by water content. The shift of this peak to more positive potential in the absence of water suggests an overpotential for the isoenergetic occupation of traps when water is present, similar to what was observed for anatase TiO_2.[32] Note that the position of the positive potential SEPL peak in dry ACN is close to 1.5 V above the valence band, matching the energy of the PL transition. The SEPL scan in dry ACN was also repeated after the addition of 4% by volume dry ethanol (EtOH) as shown in Figure 4 for the H350 sample. Similar results were obtained for the pristine sample in dry ACN and ACN with EtOH added, shown in Figure S7 of the SI. It is apparent that the intensity of PL at all potentials is diminished in the presence of EtOH, consistent with efficient scavenging of VB holes. The effect of EtOH on the intensity of near-IR PL is further evidence that the PL results from recombination of trapped electrons with VB holes. The small peak in the SEPL at positive potential for the sample containing a small amount of EtOH is shifted a few hundred mV positive of the corresponding (larger) peak in the SEPL for dry ACN electrolyte. The enhanced rate of hole scavenging in the presence of EtOH translates into the need to raise E_F to a higher value before nonradiative recombination outcompetes the weak PL.

The comparison of SEPL measurements in nonaqueous and aqueous electrolyte may be highlighting a significant difference in electron transport in RNWs in contact with a bulk aqueous solvent compared to bulk acetonitrile. As we observed previously in anatase, there appears to be an impediment for electrically occupying electron traps in aqueous solutions unless the Fermi level is high enough to access shallow electron traps within a couple hundred millivolts of the CB. We see this in Figure 2 where there is only a plateau of PL intensity at positive potentials where the electron traps should be detected. The applied potential has no effect on the PL until reaching approximately 500 mV below the conduction band edge in aqueous solution. When the electrons from the potentiostat reach the level of these shallow traps, they are then more mobile and can diffuse rapidly away and decay either nonradiatively with VB holes or into the midband gap trap states. This results in the overall increase in PL at applied potentials slightly below the CB in aqueous solution. In comparison, in ACN solution, electrons from the potentiostat are readily able to occupy trap states when the applied potential reaches the trap state energy level. The second PL increase seen in Figure 3, just below the CB, is assigned to the same process

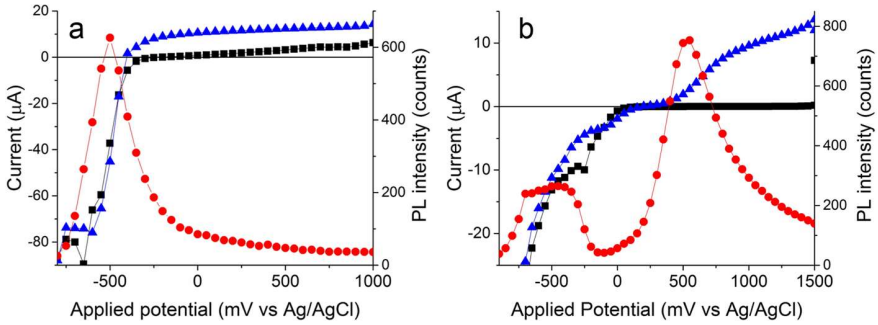

Figure 5. Currents for dark and illuminated samples overlaid with PL intensity for H350 rutile NW in (a) 0.2 M $NaClO_4$ pH 9.5 water and (b) 0.2 M $NaClO_4$ ACN. The red circles represent the intensity of PL at 835 nm, black squares are current measured in the dark, and blue triangles are current measured during the PL experiments with illumination by 350 nm light at 0.1 W/cm^2.

DOI: 10.1021/acs.jpcc.5b11231
J. Phys. Chem. C 2016, 120, 3530−3541

as described for aqueous solution above; i.e., inelastic capture of mobile electrons by traps. The decrease in PL as the Fermi level (E_F) is moved above the energy of the deep or shallow traps results from the decreased rate of occupying traps as compared to the rate of nonradiative decay, which increases as electrons are accumulated. Enhanced occupation of the luminescent (deeper) trap when E_F overlaps the shallow trap distribution is consistent with participation of the latter in trap-mediated transport.

The complete absence of the peak at positive potential for water but not for wet or dry ACN could result from water photooxidation which competes effectively for the VB holes required for PL. However, water is well-known to adsorb strongly on the TiO_2 surface, so photooxidation could have also taken place in the presence of ACN. This question is addressed below by examination of the potential dependence of photocurrents.

In all of the above PL measurements, the steady-state current was recorded at each potential along with the PL spectrum. The current was measured both under illumination from the laser and for the sample in the dark. The difference between the current for the illuminated and dark sample is the photocurrent. For example, the behavior of current for the illuminated and dark samples in relation to PL for H350 rutile is shown in Figure 5. For the aqueous sample, Figure 5a, the photocurrent decreases at a potential near where the PL is reaching a maximum, namely, − 0.5 V vs Ag/AgCl for pH 9.5. In ACN, Figure 5b, the photocurrent decreases between +0.75 and +0.5 V vs Ag/AgCl, concurrent with the maximum in PL. The photocurrent is present mainly at positive potentials, consistent with the presence of photooxidation. We observe a competition for photogenerated holes between photooxidation and PL. For example, in ACN, photooxidation of surface species by VB holes is occurring at the most positive potentials until raising the Fermi level results in the midbandgap traps being filled and many more electrons begin competing for mobile holes near the surface. In water, the photooxidation by VB holes continues until much more negative potentials because the potentiostat is not able to access midbandgap traps until the Fermi level nears the CB, thus there is little competition for VB holes for a much wider range of potentials in water compared to in ACN.

In the absence of incident light, only cathodic current is observed as expected for an n-type semiconductor. The potential at which the current changes sign when the sample is illuminated is close to the onset potential for the dark cathodic current. When there is no reversible redox couple present in the electrolyte, the photocurrent onset potential is controlled by the kinetics of charge exchange at the interface.[55] In the presence of efficient hole scavengers, the onset potential of the photocurrent is often taken to represent the flatband potential V_{fb}.[56,57] In nanosized particles lacking a space-charge layer, V_{fb} is equal to the potential at the minimum of the conduction band E_{CB}. (It is widely assumed that a negligible space-charge layer exists for moderately doped nanoparticles immersed in electrolyte solution. While the donor densities N_D of our samples may be large enough to support a space charge layer in the radial direction,[8,9] we do not have accurate knowledge of N_D and are unable to calculate the difference between the conduction band minimum and the flatband potential.) It is apparent for the SEPL in aqueous electrolyte that the onset potential for photocurrent is a few hundred mV less negative than the pH-dependent CB potential, E_{CB}. In ACN electrolyte, the difference is larger, and the photocurrent onset potential occurs at about 400 mV, about 1000 mV less negative than E_{CB}. The inefficient scavenging of holes by residual or bulk water translates into a kinetic competition between recombination and photooxidation which controls the onset potential for the photocurrent.

The above results comparing currents for the dark and illuminated samples were repeated using voltage sweeps at 100 mV/s, as shown in Figure 6a–e. The scans were done from positive to negative potentials to mimic the process used for potential-dependent PL measurements. In the voltage sweep results for a pristine RNW sample, Figure 6a,b, we see almost no photocurrent in aqueous or ACN solutions, which is consistent with the near-zero IPCE at 350 nm for pristine samples shown in ref 6. For the H350 sample in aqueous solution, Figure 6c, there is photocurrent until approximately −400 mV. For both H350 and H450 in ACN, Figure 6d,f, there is always a decrease in photocurrent where the PL reaches a maximum at +500 mV vs Ag/AgCl. For the illuminated sample, the current in the presence of ACN goes to zero at about +500 mV for H350 (Figure 6d) and +800 mV for H450 (Figure 6f), but in both cases the photocurrent, defined as the difference between the light and dark currents, goes to zero at about +500 mV. In the aqueous samples, the potential of the zero crossing of the current for the illuminated sample is also more positive for H450 (Figure 6e) than H350 (Figure 6c), despite that the zero crossing is identical for H350 and H450 in steady state photocurrent measurements. We speculate that these observations result from kinetic effects on the time scale of the voltage

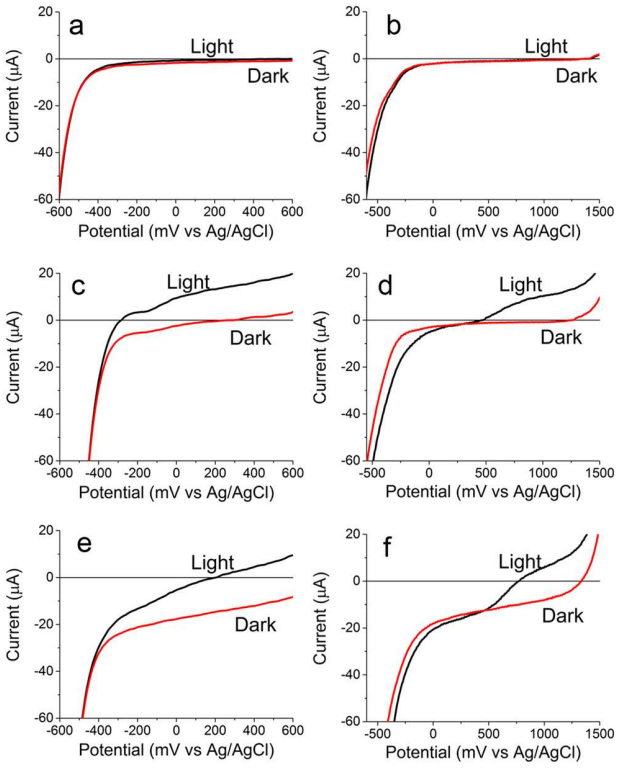

Figure 6. Voltammograms of currents in rutile nanowires in the dark and under illumination. Pristine in water (a) and ACN (b), H350 in water (c) and ACN (d), and H450 in water (e) and ACN (f). Note that only the scan from positive to negative (cathodic scan) is shown, for clarity.

DOI: 10.1021/acs.jpcc.5b11231
J. Phys. Chem. C 2016, 120, 3530−3541

sweep. Significant dark cathodic current in the H450 sample, of unknown origin, appears to add to the current for the illuminated sample. However, for both H350 and H450, currents for the dark and illuminated sample coincide at potentials less than +500 mV in ACN and −400 mV in water, similar to the steady state data in Figure 5. This is in keeping with the perception that transport and thus isoenergetic occupation of deep traps is sluggish in water as compared to ACN. While we can only monitor the luminescent traps directly, nonluminescent traps can promote nonradiative recombination. If these are also more difficult to populate in the presence of water, as the applied potential is made more negative, this would explain the extended potential range for which photooxidation can outcompete recombination. In the presence of ACN, the coincidence in the decrease in the magnitude of the anodic photocurrent with the SEPL peak at about 500 mV reveals that the luminescent transition and photooxidation compete for VB holes. The potential at which the photocurrent eventually goes to zero is that for which the rate of recombination begins to exceed that at which holes are scavenged by water or other reductants. In water as compared to ACN, inefficient isoenergetic occupation of deep traps, whether they are luminescent or not, results in less competition for holes and an extended potential range for the photocurrent.

One may ask why there would be any oxidation occurring in the ACN solutions. As we mentioned earlier, there is trace water in our ACN solutions made with $NaClO_4$ so it is possible the current is due to oxidation of residual water. This trace water could contribute to photocurrent but not drastically influence electron transport as seen in the potential-dependent PL measurements when bulk water is present. However, the magnitude of the photocurrent for the same incident laser power is similar for water, wet ACN and dry ACN electrolytes, suggesting that surface species rather than bulk water are being photooxidized. We note that the incident light flux is on the order of 10^{14} photons/sec and the measured current is on the order of 10^{14} electrons/sec, implying a nearly 100% quantum efficiency of photooxidation in all samples. Capture of holes by chemisorbed water and hydroxyl groups on the surface may contribute in to the photocurrent in all cases.

SUMMARY

Figure 7 presents our model for the PL of rutile nanowires. Significantly, the near-IR PL is assigned to the radiative recombination of trapped electrons with valence band holes. The SEPL results enable the approximate electrochemical energy of the trap state in the presence of acetonitrile to be specified, as shown in the figure. In contrast, a large overpotential is required to occupy the trap in aqueous media. The inverse relation between near-IR PL and anodic photocurrent results from competition for valence band holes. Inefficient isoenergetic trapping of electrons in the presence of bulk water results in photocurrents which persist over larger potential ranges as compared to acetonitrile electrolyte. The weak green PL appears to be the same as observed in anatase[11,31,32,34] in the presence of hole scavengers and at applied potentials near that of the CB edge. As discussed further below, we tentatively assign this visible PL to recombination of mobile electrons with trapped holes associated with oxygen vacancies.

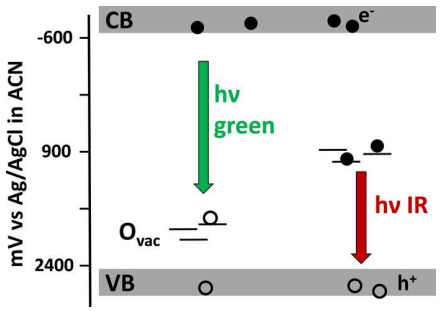

Figure 7. Scheme of proposed locations and identities of luminescent traps in rutile TiO_2.

The question remains as to the nature of the chemical species responsible for trapped electrons. Any model for the near-IR electronic transition must explain why the PL spectrum itself does not change with pH despite the Nernstian shift in the potential for occupying the luminescent trap. We must also explain why stronger near-IR PL of rutile nanowires is observed in the presence of O_2 from air compared to argon, while no difference is seen in the weak green PL. H-treatment is thought to increase oxygen vacancies, introducing color centers where one or two electrons are trapped. In addition, each bridging oxygen removed can lead to two adjacent Ti^{3+} centers. Since the near-IR PL does not increase in intensity on H-treatment, we do not think it is associated with oxygen vacancies of this type. Rather, the weak green PL, similar in shape to the component at that wavelength in anatase, appears to be related to oxygen vacancies and exhibits a weak tendency to increase in intensity on going from pristine to H350 to H450. Variations in SEPL response of the green PL correlate to the capacity of water and O_2 to bind at surface oxygen vacancies, making the green PL and its potential dependence less reproducible than that of the near-IR PL. In the SEPL of the latter, the plateaus at positive potential do vary with sample handling, but the potentials at which peaks and dips in the PL occur are more reproducible. 5-fold coordinated titanium centers, Ti_{5c}, which make up half of the bulk terminated rutile (110) surface, could trap electrons, forming Ti^{3+}. These are known to give rise to a broad spectroelectrochemical absorption in the visible and near-IR resulting from d−d transitions. The spectrum of these Ti^{3+} centers under applied bias is similar for anatase and rutile,[30] but the PL from these same trapped electrons appears at visible wavelengths in anatase. On first glance, it may seem unlikely that the near-IR PL of rutile results from electrons trapped at Ti_{5c}^{3+}, since it is hard to rationalize why the absorption spectra of Ti_{5c}^{3+} could be the same in rutile and anatase but the PL different. However, the luminescent transition is not the reverse of the molecularly based d−d transition responsible for the spectroelectrochemical absorption spectrum, which does not change the ionization state of Ti. Rather it is the recombination of the trapped electron with the valence band holes and the energy for this recombination depends on the electrochemical potential of $Ti_{5c}^{3+/4+}$ compared to that of the valence band, which is different in rutile and anatase.

H-treatment was also shown to introduce titanol groups, Ti−OH, on the surface of RNWs. These too could trap electrons (or holes),[45] but since the near-IR PL does not increase on H-treatment and the spectrum itself is not pH-dependent, electrons localized at titanol groups are unlikely to be involved in the near-IR PL. In addition to oxygen vacancies which are well-known to give rise to donor-states which enhance transport, interstitial titanium, Ti_i, is another defect in rutile.

DOI: 10.1021/acs.jpcc.5b11231
J. Phys. Chem. C 2016, 120, 3530−3541

Wendt et al.[27] presented STM images and DFT calculations supporting the assignment of a defect state, found at about 0.85 eV below the Fermi level of rutile (110), to interstitial titanium, Ti_i. The conventional assignment of this state is to an oxygen vacancy[50] or an electron trapped at Ti as a small polaron.[58] Wendt et al.,[27] on the other hand, attribute this feature, also found on the crystallographically equivalent (101) surface of bulk anatase at a slightly different energy, to Ti_i. They report that the reduced rutile (110) surface reacts with O_2 to form Ti_i which then diffuses to the near surface. The presence of the defect state was not affected by hydration or the presence of oxygen vacancies. This appears to be the same defect state, assigned differently, reported in refs 46 and 50 to be at slightly different energies for rutile (110) and anatase (101). For example, Setvin et al.[58] found the gap state on rutile (110) to lie about 0.7 eV below E_F, while the similar state in anatase is 1.0 eV below E_F. The localization of electrons in Ti 3d orbitals, on formation of Ti^{3+}, results in substantial lattice relaxation[58] that would reasonably depend on the crystal structure. In contrast to the results of photoelectron spectroscopy, transient spectroscopy of TiO_2 nanoparticles suggests that electron traps are deeper in the rutile than in anatase.[59]

Assignment of the trapping site location to a subsurface layer would help to explain why the shape of the near-IR PL spectrum does not shift with pH in aqueous media. Alternatively, theory[60] and experiment[61] suggests that trap states for excess electrons in rutile are distributed over several Ti lattice sites. In addition to its lower energy compared to the corresponding trap state PL in anatase, the near-IR PL of rutile is relatively narrow, with a half-width at half-height of about 0.25 eV compared to about 0.8 eV for the visible PL in anatase. Spreading of the electron density as suggested by theory and experiment would translate into smaller displacements in the lattice modes upon recombination of the trapped electron with holes, leading to a more narrow Franck−Condon profile.

The pH-dependence of trap occupation onset potentials in water follows that of the conduction band. As in many metal oxides, the CB potential of TiO_2 shifts to more negative potential with increasing pH,[45,62] as a result of protonation and deprotonation equilibria on the surface. Further, it is known that electron trapping by TiO_2 in aqueous media is accompanied by proton insertion.[62] Partial delocalization of the trapped charge, especially to subsurface regions, would explain why the state of protonation of the surface does not shift the PL spectrum. We speculate that the proton-mediated surface properties of water in the Helmholtz and near surface region are responsible for the observed overpotential, about 1.2 V, for occupying the trap state in the presence of water. The isoenergetic occupation of traps in wet (or dry) acetonitrile, on the other hand, is facile, revealing that the overpotential in aqueous electrolyte derives from bulk properties of water near the surface. The ability of electrons from the potentiostat to reach the illuminated region of the RNW film depends on the efficiency of carrier transport from the conductive substrate to the surface traps. The ambipolar nature of the electron diffusion in nanoparticulate TiO_2[63] emphasizes the solvation of surface charges. The strong interaction of water with the TiO_2 surface could contribute to an energy barrier for transport owing to solvent reorganization.

In ref 7, weak blue PL at about 450 nm was reported to decay over a range of picosecond to nanosecond time scales, with overall slower decay in H-treated samples. The defect state responsible for this PL was assigned to an oxygen vacancy lying about 0.3 eV below the CB. In the present work, we associate the weak green PL with a peak at about 550 nm to the recombination of free electrons with oxygen vacancy-related hole traps. We have previously found that increasing the incident light intensity (using CW excitation) results in a blue shift in the PL spectrum of TiO_2 nanotubes. (See the SI of ref 64.) The higher instantaneous powers used in the measurement of the time-resolved PL in ref 7 could have resulted in the shift from 550 to 450 nm. Similarly, Fujihara et al.[65] reported PL at 450 nm in suspensions of rutile nanoparticles, obtained using pulsed UV laser excitation. The basis for this blue shift may be similar to a Burstein−Moss shift: increase in the quasi-Fermi level of electrons under high power results in a higher energy transition. In addition to a blue-shift in the PL, high excitation densities of pulsed lasers shorten the PL lifetime compared to weak excitation,[16] owing to enhanced recombination rates as the quasi-Fermi level is raised.[66] As shown in ref 16, the near-IR PL of rutile nanoparticles in air at room temperature decays on a millisecond time scale under weak excitation conditions. Decreased recombination in rutile nanowires could result in even longer lifetimes of the near-IR PL.

The failure of oxygen in air to quench the green PL of RNWs is puzzling when considered alongside the enhancement of the near-IR PL in air as compared to argon (Figure 1). If the latter effect is attributed to decreased nonradiative recombination resulting from scavenging of CB electrons by O_2, then the green PL should have been quenched by air, as it is for anatase nanoparticles. The discrepancy might be explained by a much faster decay of the green PL compared to the near-IR PL. Though the visible PL of rutile has been observed to decay on a nanosecond time scale[7,65] in pulsed laser experiments, its lifetime under weak excitation conditions is not available and would be difficult to measure due to low quantum yield. Another unknown factor is the lifetime of the PL compared to the time scale for electron scavenging. Though we cannot say with certainty that the different effect of O_2 on the green and near-IR PL of RNWs is a result of their different PL lifetimes, the low intensity of the visible PL compared to the near-IR is itself an argument for associating a shorter lifetime with the former.

Finally, we note interesting comparisons of the PL of anatase and rutile nanoparticles. Both phases have crystal structures that can be viewed as connected TiO_6 octahedra, which are more densely packed in rutile than in anatase. The similar oxygen-vacancy related PL in both rutile and anatase may reflect the localized nature of the associated oxygen vacancy defect. The near-IR PL of RNWs, on the other hand, appears to derive from electrons trapped as Ti^{3+} but not necessarily on the surface as in the case of the under-coordinated Ti centers responsible for red and yellow PL of anatase. This conclusion derives from the very weak dependence of the near-IR PL of rutile nanoparticles on contacting solvent, as compared to strong solvent dependence for anatase visible PL.[11] The electron traps in rutile are deeper than those in anatase both in an energetic and spatial sense.

CONCLUSIONS

The photooxidation of water by rutile nanowires is the result of transfer of valence band, rather than trapped, holes. Improved transport properties rather than differences in trap state distributions are the basis for the superior performance of H-treated nanowires compared to pristine nanowires. The near-IR PL of the nanowire samples reveals that the transition results

DOI: 10.1021/acs.jpcc.5b11231
J. Phys. Chem. C 2016, 120, 3530−3541

from recombination of trapped electrons with valence band holes and is thus competitive with photooxidation. The intensity of this PL under Fermi level control reveals that there is a large overpotential for occupying traps in the presence of bulk water, and only a small barrier in the presence of trace water in acetonitrile electrolyte. The barrier to trap occupation in the presence of water as compared to acetonitrile may be a consequence of poor carrier transport in the former, which inhibits the isoenergetic occupation of deep traps under potentiostatic control. In acetonitrile, whether dry or containing ~0.2 M water, the isoenergetic pathway is facile, and in both acetonitrile and water conduction band electrons are efficiently captured inelastically by the electron trap responsible for near-IR PL.

■ ASSOCIATED CONTENT

Supporting Information

The Supporting Information is available free of charge on the ACS Publications website at DOI: 10.1021/acs.jpcc.5b11231.

SEM images of rutile nanowires (Figure S1); Raman spectra of rutile nanowires (Figure S2); photoluminescence spectra of pristine nanowires compared to H350 and H450 nanowires (Figure S3); Normalized PL spectra of rutile nanowires in water at different applied potentials (Figure S4); Current at positive potentials versus PL in the plateau region (Figure S5); comparison of PL spectra in water and acetonitrile (Figure S6); and SEPL profiles of pristine nanowires in dry acetronitrile and ethanol/acetonitrile electrolyte (PDF)

■ AUTHOR INFORMATION

Corresponding Author

* E-mail: jmchale@wsu.edu. Phone: (+01)-509-335-4063.

Notes

The authors declare no competing financial interest.

■ ACKNOWLEDGMENTS

The authors would like to acknowledge the use of the Franceschi Microscopy & Imaging Center at Washington State University for electron microscopy work. The support of the National Science Foundation (DMR-1305592) is gratefully acknowledged. J.Z.Z. acknowledges support from the BES Division of the U.S. DOE and UC MEXUS/CONACYT.

■ REFERENCES

(1) O'Regan, B.; Grätzel, M. A. Low-Cost, High-Efficiency Solar Cell Based on Dye-Sensitized Titanium Dioxide Films. *Nature* **1991**, *353*, 737−740.

(2) Fujishima, A.; Honda, K. Electrochemical Photolysis of Water at a Semiconductor Electrode. *Nature* **1972**, *238*, 37−38.

(3) Kapilashrami, M.; Zhang, Y.; Liu, Y. S.; Hagfeldt, A.; Guo, J. Probing the Optical Property and Electronic Structure of TiO_2 Renewable Energy Applications. *Chem. Rev.* **2014**, *114*, 9662−9707.

(4) Ohno, T.; Sarukawa, K.; Matsumura, M. Crystal Faces of Rutile and Anatase TiO_2 Particles and Their Roles in Photocatalytic Reactions. *New J. Chem.* **2002**, *26*, 1167−1170.

(5) Chen, H.; Nanayakkarra, C. E.; Grassian, V. H. Titanium Dioxide Photocatalysis in Atmospheric Chemistry. *Chem. Rev.* **2012**, *112*, 5919−5948.

(6) Wang, G.; Wang, H.; Ling, Y.; Tang, Y.; Yang, X.; Fitzmorris, R. C.; Wang, C.; Zhang, J. Z.; Li, Y. Hydrogen-Treated TiO_2 Nanowire Arrays for Photoelectrochemical Water Splitting. *Nano Lett.* **2011**, *11*, 3026−3033.

(7) Wheeler, D. A.; Ling, Y.; Dillon, R. J.; Fitzmorris, R. C.; Dudzik, C. G.; Zavodivker, L.; Rajh, T.; Dimitrijevic, N. M.; Millhauser, G.; Bardeen, C.; et al. Probing the Nature of Bandgap States in Hydrogen-Treated TiO_2 Nanowires. *J. Phys. Chem. C* **2013**, *117*, 26821−26830.

(8) Pesci, F. M.; Wang, G.; Klug, D. R.; Li, Y.; Cowan, A. J. Efficient Suppression of Electron-Hole Recombination in Oxygen-Deficient Hydrogen-Treated TiO_2 Nanowires for Photoelectrochemical Water Splitting. *J. Phys. Chem. C* **2013**, *117*, 25837−25844.

(9) Bisquert, J.; Garcia-Belmonte, G.; Fabregat-Santiago, F. Modeling the Electrical Potential Distribution in Nanoporous Semiconductor Electrodes. *J. Solid State Electrochem.* **1999**, *3*, 337−347.

(10) Addiss, R. R., Jr.; Ghosh, A. K.; Wakim, F. G. Thermally Stimulated Currents and Luminescence in Rutile. *Appl. Phys. Lett.* **1968**, *12*, 397−400.

(11) Knorr, F. J.; Mercado, C. C.; McHale, J. L. Trap-State distributions and Carrier Transport in Pure and Mixed-Phase TiO_2: Influence of Contacting Solvent and Interphasial Electron Transfer. *J. Phys. Chem. C* **2008**, *112*, 12786−12794.

(12) Nakamura, R.; Okamura, T.; Ohashi, N.; Imanishi, A.; Nakato, Y. Molecular Mechanisms of Photoinduced Oxygen Evolution, PL Emission, and Surface Roughening at Atomically Smooth (110) and (100) *n*-TiO_2 (Rutile) Surfaces in Aqueous Acidic Solutions. *J. Am. Chem. Soc.* **2005**, *127*, 12975−12983.

(13) Hoffmann, M. R.; Martin, S. T.; Choi, W.; Bahnemann, D. W. Environmental Applications of Semiconductor Photocatalysis. *Chem. Rev.* **1995**, *95*, 69−96.

(14) Anpo, M.; Shima, T.; Kubokawa, Y. ESR and Photoluminescence Evidence for the Catalytic Formation of Hydroxyl Radicals on Small TiO_2 Particles. *Chem. Lett.* **1985**, *14*, 1799−1802.

(15) Imanishi, A.; Fukui, K. Atomic-scale Local Structure of TiO_2 and its Influence on the Water Photooxidation Process. *J. Phys. Chem. Lett.* **2014**, *5*, 2108−2117.

(16) Wang, X.; Feng, Z.; Shi, J.; Jia, G.; Shen, S.; Zhou, J.; Li, C. Trap States and Carrier Dynamics of TiO_2 Studied by Photoluminescence Spectroscopy Under Weak Excitation Condition. *Phys. Chem. Chem. Phys.* **2010**, *12*, 7083−7090.

(17) Villareal, T. L.; Gómez, R.; González, M.; Salvador, P. A Kinetic Model for Distinguishing between Direct and Indirect Hole Transfer in the Heterogeneous Photooxidation of Dissolved Organics on TiO_2 Nanoparticle Suspensions. *J. Phys. Chem. B* **2004**, *108*, 20278−20290.

(18) Mora-Seró, I.; Villareal, T. L.; Bisquert, J.; Pitarch, A.; Gómez, R.; Salvador, P. Photoelectrochemical Behavior of Nanostructured TiO_2 Thin-Film Electrodes in Contact with Aqueous Electrolytes Containing Dissolved Pollutants: A Model for Distinguishing between Direct and Indirect Hole Transfer from Photocurrent Measurements,. *J. Phys. Chem. B* **2005**, *109*, 3371−3380.

(19) Gerischer, H. The Impact of Semiconductors on the Concepts of Electrochemistry. *Electrochim. Acta* **1990**, *35*, 1677−1699.

(20) Watson, D. F.; Meyer, G. J. Electron Injection at Dye-sensitized Semiconductor Electrodes. *Annu. Rev. Phys. Chem.* **2005**, *56*, 119−366.

(21) Cowan, A. J.; Tang, J.; Leng, W.; Durrant, J. R.; Klug, D. R. Water Splitting by Nanocrystalline TiO_2 in a Complete Photoelectrochemical Cell Exhibits Efficiencies Limited by Charge Recombination. *J. Phys. Chem. C* **2010**, *114*, 4208−4214.

(22) Swierk, J. R.; Mallouk, T. Design and Development of Photoanodes for Water-Splitting Dye-Sensitized Photoelectrochemical Cells. *Chem. Soc. Rev.* **2013**, *42*, 2357−2387.

(23) Gopal, N. O.; Lo, H.-H.; Sheu, S.-C.; Ke, S.-C. A Potential Site for Trapping Photogenerated Holes on Rutile TiO_2 Surface as Revealed by EPR Spectroscopy: An Avenue for Enhancing Photocatalytic Activity. *J. Am. Chem. Soc.* **2010**, *132*, 10982−10983.

(24) Szczepankiewicz, S. H.; Colussi, A. J.; Hoffmann, M. R. Infrared Spectra of Photoinduced Species on Hydroxylated Titania Surfaces. *J. Phys. Chem. B* **2000**, *104*, 9842−9850.

(25) Deskins, N. A.; Rousseau, R.; Dupuis, M. Distribution of Ti^{3+} Surface Sites in Reduced TiO_2. *J. Phys. Chem. C* **2010**, *114*, 5891−5897.

(26) Wang, Z.; Wen, B.; Hao, Q.; Liu, L.-M.; Zhou, C.; Mao, X.; Lang, X.; Yni, W.-J.; Dai, D.; Selloni, A.; Yang, X. Localized Excitation

DOI: 10.1021/acs.jpcc.5b11231
J. Phys. Chem. C 2016, 120, 3530−3541

of Ti^{3+} Ions in the Photoabsorption and Photocatayltic Activity of Reduced Rutile TiO_2. *J. Am. Chem. Soc.* **2015**, *137*, 9146−9152.
(27) Wendt, S.; Sprunger, P. T.; Lira, E.; Madsen, G. K. H.; Li, Z.; Hanson, J. Ø.; Matthiesen, J.; Blekinge-Rasmussen, A.; Laegsgaard, E.; Hammer, B.; et al. The Role of Interstitial Sites in the Ti3d Defect State in the Band Gap of Titania. *Science* **2008**, *320*, 1755−1759.
(28) Henderson, M. A.; Epling, W. S.; Peden, C. H. F; Perkins, C. L. Insights into Photoexcited Electron Scavenging Processes on TiO_2 Obtained from Studies of the Reaction of O_2 with OH Groups Adsorbed at Electronic Defects on TiO_2(110). *J. Phys. Chem. B* **2003**, *107*, 534−545.
(29) Yoon, Y.; Du, Y.; Garcia, J. C.; Zhu, Z.; Wang, Z.-T.; Petrik, N. G.; Kimmel, G. A.; Dohnalek, Z.; Henderson, M. A.; Rousseau, R.; et al. Anticorrelation Between Surface and Subsurface Defects and the Impact on the Redox Chemistry of TiO_2(110). *ChemPhysChem* **2015**, *16*, 313−321.
(30) Berger, T.; Anta, J. A.; Morales-Flórez, V. Spectroscopic Properties of Electrochemically Populated States of TiO_2 Films: Anatase versus Rutile. *Phys. Chem. Chem. Phys.* **2013**, *15*, 13790−13795.
(31) Knorr, F. J.; McHale, J. L. Spectroelectrochemical Photoluminescence of Trap States of Nanocrystalline TiO_2 in Aqueous Media. *J. Phys. Chem. C* **2013**, *117*, 13654−13662.
(32) Rex, R. E.; Knorr, F. J.; McHale, J. L. Surface Traps of TiO_2 Nanosheets and Nanoparticles as Illuminated by Spectroelectrochemical Photoluminescence. *J. Phys. Chem. C* **2014**, *118*, 16831−16841.
(33) Jacobsson, T. J.; Edvinsson, T. A. Spectroelectrochemical Method for Locating Fluorescent Trap States in Nanoparticles and Quantum Dots. *J. Phys. Chem. C* **2013**, *117*, 5497−5504.
(34) Mercado, C. C.; Seeley, Z.; Bandyopadhyay, A.; Bose, S.; McHale, J. L. Photoluminescence of Dense Nanocrystalline Titanium Dioxide Thin Films: Effect of Doping and Thickness in Relation to Gas Sensing. *ACS Appl. Mater. Interfaces* **2011**, *3*, 2281−2288.
(35) Mercado, C. C.; Knorr, F. J.; McHale, J. L.; Usmani, S. M.; Ichimura, A. S.; Saraf, L. V. Location of Hole and Electron Traps on Nanocrystalline TiO_2. *J. Phys. Chem. C* **2012**, *116*, 10796−10804.
(36) McHale, J. L.; Knorr, F. J. Photoluminescence and Carrier Transport in Nanocrystalline TiO_2. In *Handbook of Luminescent Semiconductor Materials*; Taylor and Francis: London, 2011; Chapter 13.
(37) Imanishi, A.; Okamura, T.; Ohashi, M.; Nakamura, R.; Nakato, T. Mechanism of water photooxidation at atomically flat TiO_2 (Rutile) (110) and (100) Surfaces. *J. Am. Chem. Soc.* **2007**, *129*, 11569−11578.
(38) Rich, C. C.; Knorr, F. J.; McHale, J. L. Trap State Photoluminescence of Nanocrystalline and Bulk TiO_2. Implications for Carrier Transport. *MRS Online Proc. Libr.* **2010**, *1268*, EE03−08/1−6.
(39) Carter, E.; Carley, A. F.; Murphy, D. M. Evidence for O_2^- Radical Stabilization at Surface Oxygen Vacancies on Polycrystalline TiO_2. *J. Phys. Chem. C* **2007**, *111*, 10630−10638.
(40) Petrik, N. G.; Kimmel, G. A. Reaction Kinetics of Water Molecules with Oxygen Vacancies on Rutile TiO_2(110). *J. Phys. Chem. C* **2015**, *119*, 23059−23067.
(41) Weidmann, J.; Dittrich, Th.; Konstantinova, E.; Lauermann, I.; Uhlendorf, I.; Koch, F. Influence of Oxygen and Water Related Surface Defects on the Dye-Sensitized TiO_2 Solar Cell. *Sol. Energy Mater. Sol. Cells* **1999**, *56*, 153−165.
(42) Peiró, A. M.; Colombo, C.; Doyle, G.; Nelson, J.; Mills, A.; Durrant, J. R. Photoinduced Reduction of Oxygen Adsorbed to Nanocrystalline TiO_2 Films: A Transient Absorption and Oxygen Scavenging Study of Different TiO_2 Preparations. *J. Phys. Chem. B* **2006**, *110*, 23255−23263.
(43) Murata, C.; Yoshida, H.; Kumagai, J.; Hattori, T. Active Sites and Active Oxygen Specia for Photocatalytic Epoxidation of Propene by Molecular Oxygen over TiO_2-SiO_2 Binary Oxides. *J. Phys. Chem. B* **2003**, *107*, 4364−4373.
(44) Henderson, M.; Epling, W. S.; Perkins, C. L.; Peden, C. H. F.; Diebold, U. Interaction of Molecular Oxygen with Vacuum-Annealed TiO_2(110) Surface: Molecular and Dissociative Channels. *J. Phys. Chem. B* **1999**, *103*, 5328−5337.
(45) Boschloo, G.; Fitzmaurice, D. Electron Accumulation in Nanostructured TiO_2 (Anatase) Electrodes. *J. Phys. Chem. B* **1999**, *103*, 7860−7868.
(46) Kavan, L.; Grätzel, M.; Gilbert, S. E.; Klemenz, C.; Scheel, H. J. Electrochemical and Photoelectrochemical Investigation of Single-Crystal Anatase. *J. Am. Chem. Soc.* **1996**, *118*, 6716.
(47) Kullgren, J.; Aradi, B.; Frauenheim, T.; Kavan, L.; Deák, P. Resolving the Controversy about the Band Alignment between Rutile and Anatase: The Role of OH^-/H^+ Adsorption. *J. Phys. Chem. C* **2015**, *119*, 21952−21958.
(48) Yamakata, A.; Ishibashi, T.; Onishi, H. Effects of Accumulated Electrons on the Decay Kinetics of Photogenerated Electrons in Pt/TiO_2 Photocatalyst Studied by Time-Resolved Infrared Absorption. *J. Photochem. Photobiol., A* **2003**, *160*, 33−36.
(49) Mandal, D.; Hamann, T. W. Band Energies of Nanoparticle Semiconductor Electrodes Determined by Spectroelectrochemical Measurements of Free Electrons. *Phys. Chem. Chem. Phys.* **2015**, *17*, 11156−11160.
(50) Thomas, A. G.; Flavell, W. R.; Mallick, A. K.; Kumarasinghe, A. R.; Tsoutsou, D.; Khan, N.; Chatwin, C.; Rayner, S.; Smith, G. C.; Stockbauer, R. L.; et al. Comparison of the Electronic Structure of Anatase and Rutile TiO_2 Single-Crystal Surfaces Using Resonant Photoemission and X-Ray Absorption Spectroscopy. *Phys. Rev. B: Condens. Matter Mater. Phys.* **2007**, *75*, 035105/1−12.
(51) Yang, Y.; Ling, Y.; Wang, G.; Liu, T.; Wang, F.; Zhai, T.; Tong, Y.; Li, Y. Photohole Induced Corrosion of Titanium Dioxide: Mechanism and Solutions. *Nano Lett.* **2015**, *15*, 7051−7057.
(52) Pu, Y.-C.; Ling, Y.; Chang, K.-D.; Liu, C.-M.; Zhang, J.-Z.; Hsu, Y.-J.; Li, Y. Surface Passivation of TiO_2 Nanowires Using a Facile Precursor Treatment Approach for Photoelectrochemical Water Oxidation. *J. Phys. Chem. C* **2014**, *118*, 15086−15094.
(53) She, C.; Guo, J.; Lian, T. Comparison of Electron Injection Dynamics from Re-bipyridyl Complexes to TiO_2 Nanocrystalline Thin Films in Different Solvent Environments. *J. Phys. Chem. B* **2007**, *111*, 6903−6912.
(54) Redmond, G.; Fitzmaurice, D. Spectroscopic Determination of Flatband Potentials for Polycrystalline TiO_2 Electrodes in Nonaqueous Solvents. *J. Phys. Chem.* **1993**, *97*, 1426−1430.
(55) Berger, T.; Monllor-Satoca, D.; Jankulovska, M.; Lana-Villareal, T. The Electrochemistry of Nanostructured Titanium Dioxide Electrodes. *ChemPhysChem* **2012**, *13*, 2824−2875.
(56) Bedja, I.; Hotchandani, S.; Kamat, P. V. Preparation and Photoelectrochemical Characterization of Thin SnO_2 Nanocrystalline Semiconductor Films and Their Sensitization with bis(2,2′-bipyridine)(2,2′-bipyridine-4,4′-cicarboxylic acid)ruthenium complex. *J. Phys. Chem.* **1994**, *98*, 4133−4144.
(57) Kavan, L.; Kratochvilová, K.; Grätzel, M. Study of Nanocrystalline TiO_2 (Anatase) in the Accumulation Region. *J. Electroanal. Chem.* **1995**, *394*, 93−102.
(58) Setvin, M.; Franchini, C.; Hao, X.; Schmid, M.; Janotti, A.; Kaltak, M.; Van de Walle, C. G.; Kresse, G.; Diebold, U. Direct View of Excess Electrons in TiO_2 Rutile and Anatase. *Phys. Rev. Lett.* **2014**, *113*, 086402/1−5.
(59) Yamakata, A.; Vequizo, J. J. M.; Matsunaga, H. Distinctive Behavior of Photogenerated Electrons and Holes in Anatase and Rutile TiO_2 Powders. *J. Phys. Chem. C* **2015**, *119*, 24538−24545.
(60) Deskins, N. A.; Rousseau, R.; Dupuis, M. Distribution of Ti^{3+} Surface Sites in Reduced TiO_2. *J. Phys. Chem. C* **2010**, *114*, 5891−5897.
(61) Zhang, Z.; Cao, K.; Yates, J. T., Jr. Defect-Electron Spreading on the TiO_2(110) Semiconductor Surface by Water Absorption. *J. Phys. Chem. Lett.* **2013**, *4*, 674−679.
(62) Lyon, L. A.; Hupp, J. T. Energetics of Nanocrystalline Titanium Dioxide/Aqueous Solution Interfaces: Approximate Conduction Band Edge Variations between $H_0 = -10$ and $H_- = +26$. *J. Phys. Chem. B* **1999**, *103*, 4623−4628.

DOI: 10.1021/acs.jpcc.5b11231
J. Phys. Chem. C 2016, 120, 3530−3541

(63) Kopidakis, N.; Schiff, E. A.; Park, N.-G.; van de Lagemaat, J.; Frank, A. J. Ambipolar Diffusion of Photocarriers in Electrolyte-Filled Nanoporous TiO_2. *J. Phys. Chem. B* **2000**, *104*, 3930−3936.
(64) Mercado, C. C.; Knorr, F. J.; McHale, J. L. Observation of Charge Transport in Single Titanium Dioxide Nanotubes by Micro-Photoluminescence Imaging and Spectroscopy,. *ACS Nano* **2012**, *6*, 7270−7280.
(65) Fujihara, K.; Izumi, S.; Ohno, T. Time-Resolved Photoluminescence of Particulate TiO_2 Photocatalysts Suspended in Aqueous Solutions. *J. Photochem. Photobiol., A* **2000**, *132*, 99−104.
(66) Barzykin, A. V.; Tachiya, M. Mechanism of Charge Recombination in Dye-Sensitized Nanocrystalline Semiconductors: Random Flight Model. *J. Phys. Chem. B* **2002**, *106*, 4356−4363.

DOI: 10.1021/acs.jpcc.5b11231
J. Phys. Chem. C 2016, 120, 3530−3541